Biomaterial and biocompatibility evaluation of tunicate nanocellulose for tissue engineering

137 (2022) 212828

Contents lists available at ScienceDirect

Biomaterials Advances

journal homepage: www.journals.elsevier.com/materials-science-and-engineering-c

Biomaterial and biocompatibility evaluation of tunicate nanocellulose for tissue engineering

Peter Apelgren [a,b,1], Sanna Sämfors [c,1], Karin Säljö [a,b], Johan Mölne [d], Paul Gatenholm [c], Christofer Troedsson [e], Eric M. Thompson [e,f], Lars Kölby [a,b,*]

[a] Department of Plastic Surgery, Institute of Clinical Sciences, Sahlgrenska Academy, University of Gothenburg, Gothenburg, Sweden
[b] Region Västra Götaland, Sahlgrenska University Hospital, Department of Plastic Surgery, Gothenburg, Sweden
[c] 3D Bioprinting Centre, Department of Chemistry and Chemical Engineering, Chalmers University of Technology, Gothenburg, Sweden
[d] Department of Pathology, Institute of Clinical Sciences, Sahlgrenska Academy, University of Gothenburg, Gothenburg, Sweden
[e] Ocean TuniCell AS, N-5258 Blomsterdalen, Norway
[f] Department of Biological Sciences, University of Bergen, N-5006 Bergen, Norway

A B S T R A C T

Extracellular matrix fibril components, such as collagen, are crucial for the structural properties of several tissues and organs. Tunicate-derived cellulose nanofibrils (TNC) combined with living cells could become the next gold standard for cartilage and soft-tissue repair, as TNC fibrils present similar dimensions to collagen, feasible industrial production, and chemically straightforward and cost-efficient extraction procedures. In this study, we characterized the physical properties of TNC derived from aquaculture production in Norwegian fjords and evaluated its biocompatibility regarding induction of an inflammatory response and foreign-body reactions in a Wistar rat model. Additionally, histologic and immunohistochemical analyses were performed for comparison with expanded polytetrafluoroethylene (ePTFE) as a control. The average length of the TNC as determined by atomic force microscopy was tunable from 3 μm to 2.4 μm via selection of a various number of passages through a microfluidizer, and rheologic analysis showed that the TNC hydrogels were highly shear-thinning and with a viscosity dependent on fibril length and concentration. As a bioink, TNC exhibited excellent rheological and printability properties, with constructs capable of being printed with high resolution and fidelity. We found that post-print cross-linking with alginate stabilized the construct shape and texture, which increased its ease of handling during surgery. Moreover, after 30 days in vivo, the constructs showed a highly-preserved shape and fidelity of the grid holes, with these characteristics preserved after 90 days and with no signs of necrosis, infection, acute inflammation, invasion of neutrophil granulocytes, or extensive fibrosis. Furthermore, we observed a moderate foreign-body reaction involving macrophages, lymphocytes, and giant cells in both the TNC constructs and PTFE controls, although TNC was considered a non-irritant biomaterial according to ISO 10993-6 as compared with ePTFE. These findings represent a milestone for future clinical application of TNC scaffolds for tissue repair.

One sentence summary: In this study, the mechanical properties of tunicate nanocellulose are superior to nanocellulose extracted from other sources, and the biocompatibility is comparable to that of ePTFE.

1. Introduction

Extracellular matrices comprising collagen fibrils and proteoglycans are critical for providing the structural properties of several tissues and organs, such as skin, cartilage, adipose tissue, and blood vessels. They also play an important role in organizing the inorganic phase in hard tissue, such as bone. There is a continuous search for the ideal scaffold for tissue engineering and regenerative medicine. Because several applications are currently being translated to the clinic, researchers now focus on processability and biocompatibility. Nanocellulose is an attractive scaffold component for tissue repair because of its high degree of cytocompatibility, biocompatibility, and similarity to native collagen [1]. Nanocellulose mainly originating from bacteria, algae, and wood has been used as scaffolding biomaterial in tissue engineering over the previous decade. To date, bacterial cellulose/nanocellulose has been preferred for the development of biomedical applications, including those focused on cartilage repair [2–4], for the following reasons: 1) compared with plant-derived nanocellulose, bacterial nanocellulose does not contain contaminating compounds, such as lignin and hemicelluloses, and can, therefore, be produced at higher purity and with greater compositional reliability; and 2) the physicochemical properties of bacterial nanocellulose are superior to plant-based sources, as they

* Corresponding author at: Department of Plastic Surgery, Institute of Clinical Sciences, Sahlgrenska Academy, University of Gothenburg, Gothenburg, Sweden.
E-mail address: lars.kolby@surgery.gu.se (L. Kölby).
[1] These authors contributed equally to this work.

https://doi.org/10.1016/j.bioadv.2022.212828
Received 14 January 2022; Received in revised form 6 April 2022; Accepted 21 April 2022
Available online 5 May 2022

have a higher aspect ratio, higher crystallinity, and fibril dimensions that resemble those of human collagen. However, production of bacterial nanocellulose for biomedical applications presents two important drawbacks: 1) it requires extensive perfusion with NaOH solutions to remove contaminating endotoxins [5]; and 2) despite considerable research efforts, production upscaling remains challenging.

Marine tunicates have acquired the capacity to synthesize cellulose through horizontal gene transfer of a bacterial gene encoding cellulose synthase [6]. Tunicates are invertebrates with an outer covering (a "tunic") comprising tunicin (i.e., cellulose produced by tunicates) among other carbohydrates and proteins. Ascidians, a subclass of tunicates, can be grown in large quantities, thereby enabling industrial-scale production of tunicate cellulose (TC) and nanocellulose (TNC), with TC composed of nearly pure cellulose 1_β allomorph [7,8]. Tunicates have subsequently improved the physicochemical properties of bacterial nanocellulose fibrils even further, allowing achievement of the highest aspect ratios and crystallinity indexes known in nature [9,10], which in turn results in excellent reinforcing-scaffolding properties for 3D organ and tissue bioprinting [11]. Homogenization with a microfluidizer has been applied for preparation of nanocellulose hydrogel derived from wood; however, bacterial cellulose cannot be processed by homogenization due to the compaction and dewatering of the bacterial membrane during processing [12]. A recent study showed that the counter-collision process can be successfully used for fibrilization of bacterial cellulose pellicle membranes [12]. Similar to bacterial nanocellulose, TC-based structures lack contaminating hemicelluloses and lignin, and TNC can be produced to very high purity [13]. Importantly, tunicate-based production of nanocellulose also addresses the two main drawbacks of bacterial nanocellulose production: it can be done at scale (Fig. 1), and it does not require extensive perfusion to eliminate contaminating endotoxins. Thus, TNC offers great potential in biomedical applications along with a reduced risk of disease transmission in clinical use as compared with bovine- or porcine-derived material (e.g., collagen) due to much larger evolutionary and environmental distances [14]. Moreover, the ocean offers sustainable, low-trophic resource alternatives for raw materials. Furthermore, the entire production value chain of TC and TNC has now been established (Fig. 2).

Understanding and evaluating the interaction between a biomaterial and living host tissues and the consequential immune responses caused by implantation are crucial in tissue engineering. The biomaterial mixed with autologous cells that subsequently proliferate, differentiate, and restore tissues should cause as little tissue disturbance as possible. Ideally, the biomaterial should only instigate a short-term inflammatory response, followed by a smooth biointegration process. Simultaneously, the biomaterial should offer sufficiently long-term mechanical stability and cell support.

Implants of foreign materials of any kind inevitably result in some degree of immune response. The initial injury associated with surgical implantation activates the innate immune response, after which blood proteins are deposited on the biomaterial surface to create a provisional matrix (comprising cytokines and growth factors), which then regulates the subsequent inflammatory response, macrophage activity, and wound-healing properties. Acute inflammation characterized by the invasion of polymorphonuclear leukocytes (i.e., neutrophils) usually declines within 1 week [16]. The ensuing chronic inflammatory response entails the presence of mononuclear cells, such as lymphocytes and plasma cells, and typically lasts up to 4 weeks [17]. The subsequent granulation phase, including foreign-body reaction, involves the presence of macrophages, giant cells, fibroblasts, and fibrous-capsule development, and can last for years around the implanted material [18].

Polytetrafluoroethylene (PTFE) has been extensively used for medical purposes, including sutures, meshes in hernia-repair surgery, and vascular grafts/patches, and is known for its excellent mechanical properties and biocompatibility [19–24]. Other sources of nanocellulose (i.e., synthetic, bacterial, and wood nanocellulose) have been evaluated [1,5,12,25–41] using human cells; however, their biological disadvantages include inflammatory reactions caused by endotoxins, such as contamination by lipopolysaccharides and cytotoxicity caused by silica particles [35], and lignin [42]. Some of these drawbacks have been reduced by employing different purifying steps and modifications. Lin et al. [43] published a comprehensive review of different sources of nanocellulose from a biomedical perspective.

In reconstructive surgery, lost or malformed tissues pose a common challenge for the surgeon. For example, a lost breast due to cancer can be reconstructed using silicone implants or more complex surgical procedures, such as a DIEP-flap (Deep Inferior Epigastric Perforator flap); however, these procedures have both short- and long-term complications, some of which can potentially be avoided through tissue engineering. A custom-made implant of autologous adipose tissue with perfect volume and shape would revolutionize the ability to reconstruct breasts and other soft-tissue defects. Furthermore, the complex shape of the external ear could easily be reproduced by a bioprinter mirroring the contralateral auricle, whereas this shaping and carving procedure is highly challenging for the plastic surgeon. The addition of autologous chondrocytes to the bioink could potentially simplify some of the complicated steps involved in ear-reconstruction methods.

To achieve these goals, rigorous, preclinical biocompatibility testing of the used biomaterials is of critical importance and one of the endpoints of the present study. Here, we assessed the physical properties of TNC and evaluated the biocompatibility of this novel biomaterial in order to promote its possible translation to the clinic for tissue repair.

2. Materials and methods

2.1. TNC production

The marine tunicate species *Ciona intestinalis* was grown in an aquaculture system with natural recruitment at Rong (60.4720° N,

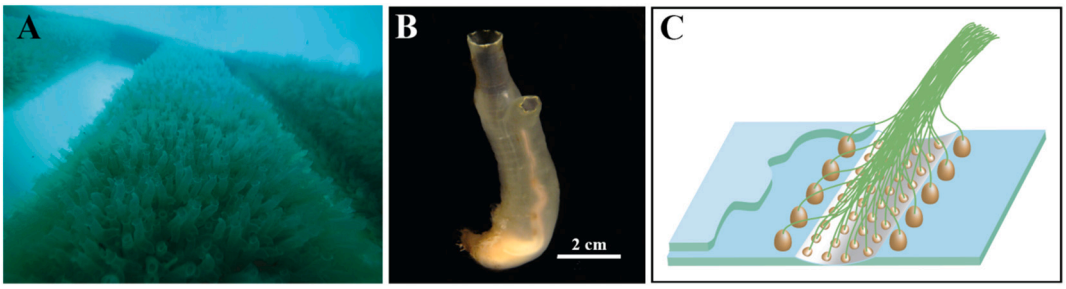

Fig. 1. Marine tunicate *Ciona intestinalis* as a source for production of high-quality nanocellulose fibrils. (A) *Ciona* are produced at scale (100 s of tons) at aquaculture facilities in Rong, Norway. (B) An individual *C. intestinalis*. The animals are typically harvested in a size range of 15–20 cm. The cellulose-rich tunic surrounds the animal (bottom), with its digestive tract and gonoducts projecting up toward the atrial siphon (right). The animal collects particles for filter-feeding through the oral siphon (top). (C) Tunicates produce cellulose fibrils through arrays of cellulose synthase terminal complexes embedded in the epidermis facing the tunic [15]. This "manufacturing" system produces 1_β allomorph cellulose with the highest crystallinity known in nature. The schematic is based on Kimura and Itoh [8].

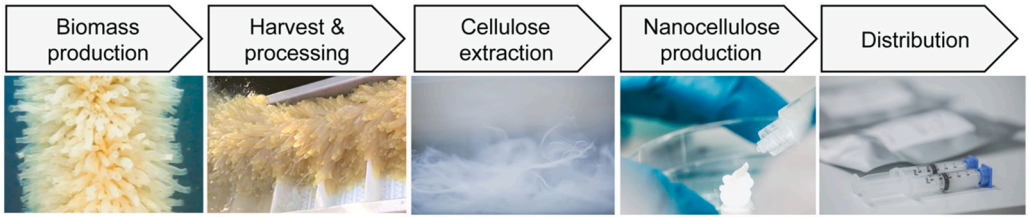

Fig. 2. The value chain for tunicate nanocellulose is now fully established from robust tunicate aquaculture to distribution of ultrapure fibrils with very low endotoxin and bioburden values that meet FDA requirements for biomedical applications. Images reproduced with permission from www.oceantunicell.com.

8.4689° E) on the west coast of Norway. After 6 to 8 months of growth, the tunicates were harvested, and the cellulose-rich outer tunics were mechanically separated from the protein- and lipid-rich inner parts. The cellulose was extracted and purified from the tunics by a modified pulping procedure [11]. The cellulose was enzymatically pre-treated (Endoglucanase Novozym 476; Novozymes AS, Bagsvaerd, Denmark) [13] and then mechanically homogenized to produce nanocellulose (TUNICELL ETC; Ocean TuniCell AS, Blomsterdalen, Norway). The final TUNICELL ETC preparations were evaluated for bioburden (bacteria and fungi) according to European Pharmacopoeia Chapter 2.6.12 and endotoxin levels (pyrogene recombinant factor c assay protocol; Lonza Group AG, Basel, Switzerland) to ensure adherence to FDA medical-grade standards. Cellulose crystallinity index was determined by X-ray diffraction according to the method described by Park et al. [44].

2.2. Hydrogel ink preparation

Lyophilized sodium alginate powder Pronova SLG100 (NovaMatrix; DuPont, Oslo, Norway) was mixed with sterile 4.6% D-mannitol aqueous solution (Sigma-Aldrich, Darmstadt, Germany) and placed on a shaking table until formation of a transparent alginate hydrogel (3%, w/v). The resulting alginate solution was mixed with 2.5% medical-grade TNC hydrogel TUNICELL ETC (Ocean Tunicell AS) by connecting two syringes with a Luer lock adapter and transferring the solutions back and forth multiple times until a homogeneous nanocellulose–alginate composite hydrogel was formed. The resulting mixture contained 80 vol% of the 2.5% nanocellulose hydrogel and 20 vol% of the 3% alginate hydrogel, which resulted in a ratio between nanocellulose and alginate of 3.33. All materials used in this process were sterile and endotoxin-free.

2.3. Bioprinting of discs

Discs for the endotoxin assay and in vivo biocompatibility study were printed using the pneumatic extrusion bioprinter BioX (CELLINK AB; Goteborg, Sweden) mounted in a laminar air flow (LAF) bench. Before printing, the printer was cleaned with 70% ethanol, followed by running a sterilizing program with ultraviolet light. Two different G-codes were used for printing either porous discs with a grid structure (10 × 10 × 1 mm) or solid discs (10 × 10 × 1.2 mm). The grids were printed in three layers using plastic dispensing tips with a gauge opening of 410 μm (CELLINK AB), with the printing pressure maintained at 16 kPa to 17 kPa throughout the printing process. After printing, the grid constructs were cross-linked in 100 mM endotoxin-free $CaCl_2$ solution for 10 min. The solid discs were cross-linked in 100 mM endotoxin-free $CaCl_2$ solution for 10 min. After cross-linking, the same number of discs of each type were chosen randomly for the endotoxin assays. These discs were washed in endotoxin-free sterile water three times and stored in water. For the in vivo biocompatibility study, the discs were washed in Hank's balanced salt solution (HBSS; Sigma-Aldrich) three times and stored in fresh HBSS until implantation. Printed, cell-free constructs for the in vivo experiment were implanted into Wistar rats within 1 h after printing.

2.4. Nanocellulose fibril characterization by atomic force microscopy (AFM)

Freshly-cleaved mica sheets were coated with a poly(ethylene imine) (Sigma-Aldrich) solution (0.1 mg/ml) by dipping the sheets in the solution for 1 min, washing in deionized (DI) water, and then air-dried inside a LAF hood. The nanocellulose-fiber dispersion was diluted 100, 1000, or 10,000 times in DI water, and a few drops of the dispersion was then placed on top of the coated mica sheets and dried inside a LAF hood.

The dried film casts were subjected to the tapping mode of a Digital Instrument Nanoscope IIIA (Digital Instruments Inc., Tonawanda, NY, USA) with a 10-nm thin tip under the silicone cantilever (NSC 15; MicroMasch OÜ, Tallinn, Estonia).

2.5. Rheological viscosity and cross-linking measurements

The viscous property of the cellulose hydrogels was analyzed using the Discovery HR-2 rheometer (TA Instruments, Crawley, UK) with a Peltier plate. The measurements were performed at 25 °C, and the samples were allowed to reach equilibrium temperature for 60 s prior to each measurement. An aluminum plate–plate (20 mm; gap = 500 μm) was used, and shear viscosity was evaluated by increasing the shear rate from 0.1/ s to 1000 s^{-1}.

Oscillation-time measurements were conducted on the different cellulose hydrogel samples at 1.5% strain and a frequency of 1 Hz for 10 min. All measurements were conducted using a plate–plate geometry of 20 mm. Hydrogel (0.15 ml) was added to the bottom plate, and the top plate was lowered slowly, leaving a gap of 500 μm. At 60 s after initiating the measurement, 1 ml of 0.1 M $CaCl_2$ was dispensed around the sample while gathering data on the storage modulus.

2.6. Viability assay using fibroblasts

Fibroblasts (Human Dermal Fibroblasts, adult) were expanded in DMEM media prior to printing. On the day of printing the cells were detached from the culture flasks using TrypLE (Thermo Fisher Scientific, Waltham, MA, USA) and resuspended in fresh DMEM media. The cell suspension was mixed with the tunicell nanocellulose/alginate mixture at a volume ratio of 1:10 by very gently pushing the mixtures back and forth in two syringes connected with a luer-lock connector several times. The resulting cell density was 1 million cells/ml of hydrogel. The cell-hydrogel was transferred to a cartridge and printed using an Inkredible 3D printer (CELLINK AB). Grids were printed using a nozzle size of 410 μm and the printing pressure was kept below 10 kPa. After printing the grids were crosslinked in 0.1 M $CaCl_2$ for 10 min, followed by rinsing in HBSS. The grids were placed in fresh DMEM media and incubated at 37 °C in 5% CO_2.

Cell viability was measured directly after printing and at day 3 of culture using an Olympus Microscope with a x10 objective. The cells were stained using a LIVE/DEAD Cell Imaging Kit (Invitrogen; Thermo Fisher Scientific), a two-component imaging kit which stains viable cells with calcein-AM and dead cells with BOBO-3 Iodine. The staining was performed in accordance to the manufacturers protocol. In brief, the printed constructs were washed with HBSS for 30 min at 37 °C. The two

different components in the LIVE/DEAD kit were mixed together to make a 2× working solution. The solution was mixed with an equal volume of HBSS and added to cover the printed constructs. The constructs were incubated for 1 h at 37 °C. The staining solution was removed and washed with HBSS for 1 h at 37 °C before imaging. Viable cells were imaged by exciting at 488 nm and the dead cells at 570 nm. Images were processed using Image J.

2.7. Bioburden and endotoxins

Printed discs were transferred to endotoxin-free tubes, and HBSS was added (0.01 ml HBSS per mg of print), followed by placement of tubes on a shaking table at 37 °C. After 1 h, the liquid was collected for endotoxin and bioburden analyses, as described.

2.8. Control biomaterial

Expanded PTFE (ePTFE; Gore Dualmesh; W.L. Gore & Associates Inc., Phoenix, AZ, USA) served as the control. The Dualmesh is a microporous biomaterial with one textured side and a smoother surface on the other side. The ePTFE sheets were 10 × 10 × 1 mm.

2.9. Animals

Eighteen female Wistar rats with a mean weight 209 ± 15 g were divided into three groups (Table 1). The fur on the back was shaved under general anesthesia (isoflurane; Piramal Critical Care, Voorschoten, Netherlands), and four identical constructs were implanted subcutaneously in four separate pockets (Fig. S1). The pockets were closed using Prolene 6-0 (Ethicon, Sommerville, NJ, USA) and sealed with wound spray (Opsite; Smith & Nephew, Watford, UK). Nine animals were euthanized at day 30 and the rest at day 90. The implants and surrounding tissues were retrieved and fixed in paraformaldehyde saturated with 20 mM $CaCl_2$, followed by sectioning and staining prior to histopathologic examination.

2.10. Histopathology

The sections were microscopically examined (Nikon Eclipse 90i epifluorescence microscope; Nikon Instruments Inc., Melville, NY, USA) and digitally scanned (Pannoramic 250 Flash; 3DHISTECH, Ltd., Budapest, Hungary). The qualitative evaluation described each implant (ePTFE; solid and gridded TNC constructs) and its immediate surroundings (i.e., reaction zone) separately. Additionally, histopathologic evaluation was semi-quantitatively performed according to the ISO 10993-6 standard [43]. The solid TNC and ePTFE sections stained with hematoxylin and eosin (H&E) were used to determine the inflammatory response, and capsule thickness (i.e., collagen content) was determined using Masson's trichrome staining. The two different surfaces of the ePTFE constructs were assessed separately, with the most reactive zone chosen on each side (i.e., that with the most cell activity) (Fig. S2). The solid TNC constructs were assessed focusing on the surface facing the fascia in order to avoid any surgery-related artefacts. The number of polymorphonuclear neutrophils, macrophages, lymphocytes, plasma cells, and giant cells present per high-power (400×) field in the most active areas was identified and manually counted. ISO assessment was performed by three observers (one pathologist and two surgeons) that discussed and scored each section together.

Table 1
Study design.

Group	Animals	Implants	Day 30 (n)	Day 90 (n)
1	6	ePTFE	12	12
2	6	TNC Grid	12	12
3	6	TNC Solid	12	12

The ePTFE and solid TNC implants provided the cross-sectional measurements of the biomaterial area and reaction-zone area, which were averaged and tabulated. The biomaterial in each section was manually circled and the area calculated in Photoshop (Adobe Systems, San Jose, CA, USA). The implant area was independently calculated twice on each section (a–d) resulting in a mean value. If the first and second areas differed by >15%, the area was measured a third time using both H&E- and Masson's trichrome-stained sections to optimize the assessment and avoid any large inconsistencies due to selection errors.

2.11. Statistical analysis

Data were presented as the mean ± standard deviation.

3. Results

3.1. Biomaterial characteristics

Enzymatically pretreated TNC (TUNICELL ETC) was consistently produced to >99% purity and 89% crystallinity (Fig. S3) in clean-room facilities. Fiber lengths versus microfluidizer cycle numbers are given in Table 2. SEM and FITR of the *Ciona intestinalis* produced nanocellulose have been previously reported [11]. Bioburden and endotoxin levels were consistently <10 CFU/ml and <0.5 EU/ml, respectively, conforming to FDA requirements for medical-grade products.

3.2. Fibril characterization and processability

The TNC hydrogel comprised a dense network of fibrils that could be visualized by AFM analysis (Fig. 3(A–C)). After a 100-fold dilution, the AFM image remained completely covered in a fibril network, with the hydrogel requiring dilution of up to 10,000-fold before individual fibrils could be visualized.

Fig. 3(D) shows an AFM image of wood nanocellulose fibrils processed with a homogenizer, revealing “fluffy” fibrils with varying size distributions. Fig. 3(B) shows an image of TNC prepared with a homogenizer using six cycles of homogenization. In contrast to wood nanocellulose, TNC fibrils were longer and presented smooth surfaces with a relatively narrow size distribution (Fig. 3(E)). Increasing the number of homogenization cycles decreased the size of the fibrils from ~3 μm after six cycles of homogenization to ~2.5 μm after 12 cycles (Fig. 4(A)). Additionally, the normal distribution indicated that increasing the cycle number decreased the variability in length to provide a more homogeneous hydrogel (Fig. 4(B)), with these decreased fibril lengths also contributing to a decrease in viscosity, which allowed extrusion of the hydrogel through a needle or a 3D-printing nozzle and requiring lower printing pressure (Table 2). Moreover, longer fibril lengths resulted in improved printing fidelity. Another way of controlling viscosity was to change the fibril concentration in the hydrogel, where larger amounts of fibers resulted in higher viscosities. The cellulose hydrogel at 2.5% had a viscosity of ~100 Pa·s, whereas an increase in the concentration to 4% increased the viscosity four-fold (Fig. 5 and Table 3).

Table 2
Effect of homogenization on TNC fibril length and viscosity according to the number of homogenization cycles.

Sample	Average length (μm, mean ± SD)	Viscosity (at shear rate 10^0 s^{-1})
TNC 6 cycles	3.03 ± 1.10	144
TNC 9 cycles	2.64 ± 0.86	147
TNC 12 cycles	2.43 ± 0.82	93

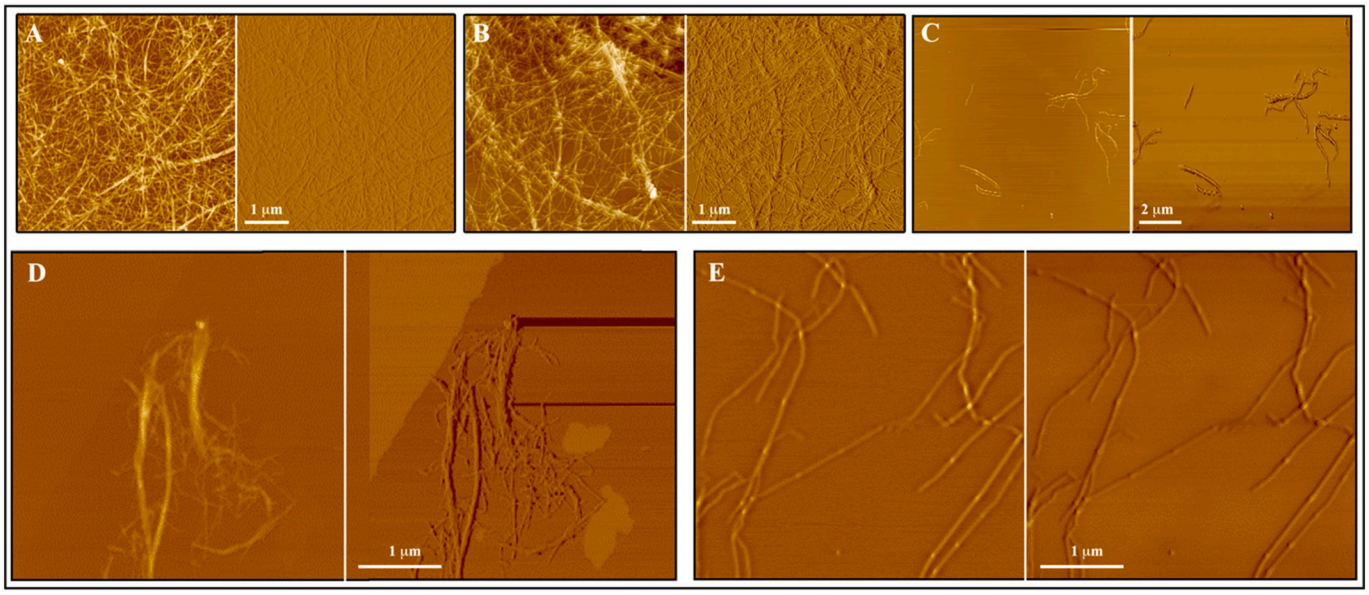

Fig. 3. AFM images. (A–C) Different dilutions of the TNC fibril dispersion after it has been dropped onto freshly-cleaved mica sheets. (A) 100-, (B) 1000-, and (C) 10,000-fold dilutions. (D, E) Cellulose nanofibrils derived from (D) wood and (E) tunicates at 10,000-fold dilutions. Bars, 1 μm (A–B and D–E) and 2 μm (C).

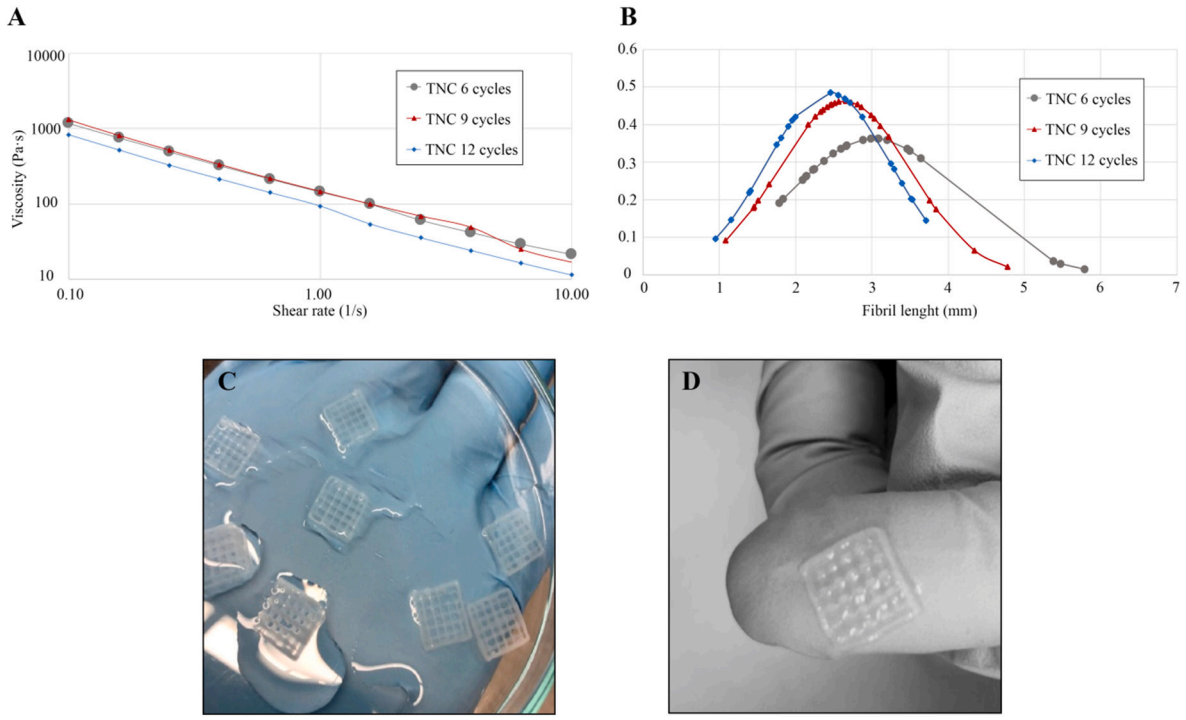

Fig. 4. Homogenization effect on the viscosity, fibril-length distribution, and printability of the TNC fibers. (A) Plot showing changes in viscosity for different amounts of homogenization cycles (6, 9, and 12 cycles) and measured with a rheometer. (B) Plot of the normal distribution of fibril length for six, nine, and 12 cycles as determined by AFM. (C, D) Grids printed from TNC/alginate hydrogels mixed with fibroblasts.

3.3. The creation of stable 3D structures from the cellulose hydrogel

To form stable 3D structures, the nanocellulose hydrogel can be mixed with alginate, which can be cross-linked using divalent cations, such as Ca^{2+}. Alginate on its own is quite brittle when crosslinked and difficult to print into 3D structures. Addition of nanocellulose allows for unique printability due to its shear thinning properties, which results in a more robust gel with increased permeability for macromolecules. When mixed at a volumetric ratio of 80:20 (TNC:alginate), the resulting cellulose/alginate hydrogel showed cross-linking ability similar to pure alginate while maintaining similar viscosities to those observed for the pure TNC hydrogel (Fig. 6 and Table 4).

3.4. Printing with cells for the live/dead assay

Cell viabilities inside the cellulose/alginate hydrogels were determined by 3D-printing fibroblasts mixed with the hydrogel, followed by cross-linking in $CaCl_2$. Viability was determined using a live/dead assay

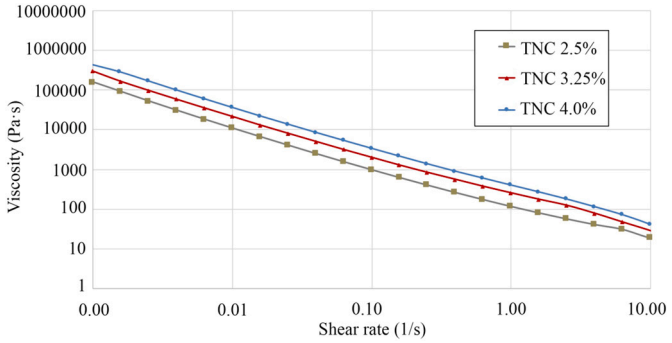

Fig. 5. The effect of TNC concentration on viscosity. Changes in viscosity according to the concentration of the TNC hydrogel as measured using a rheometer for 2.5% TNC, 3.25% TNC, and 4.0% TNC.

Table 3
Viscosity is TNC-concentration-dependent.

Sample	Viscosity (at shear rate 10^0 1/s)
TNC 2.50%	118
TNC 3.25%	258
TNC 4.00%	408

Viscosity at a shear rate of 100 s^{-1} and measured for hydrogels at different TNC concentration (2.5%, 3.25%, and 4.0%).

involving imaging of living (green) and dead (red) cells. We observed an even cell distribution throughout the printed construct, with fibroblast viability at days 0 and 3 measured at 87% and 98%, respectively.

3.5. Samples for the biocompatibility study

To assess the biocompatibility of the cellulose/alginate hydrogels, we designed two different discs for bioprinting (one solid and one porous with an internal grid structure) (Fig. 7). Both discs were printed in three layers with a diameter of 10 mm and a total height of 1.2 mm. The printed discs demonstrated good reproducibility, with an average weight for the solid discs after cross-linking of 110 ± 18.1 mg relative to 68.6 ± 3.9 mg for the gridded discs (Table 5). Stability testing of the gridded discs showed that after storage in saline solution for 5 days, the average weight had decreased to 65.0 ± 4.4 mg, indicating minimal dissociation of material from the discs during storage.

3.6. In vivo implantation and explantation of the TNC hydrogels

Wistar rats were monitored daily for post-operative complications. All 18 rats thrived throughout the study period, and the surgical wounds healed without any problems. At 3-days post-surgery, one animal (in the ePTFE group) displayed a discrete reddening in the skin around the incision, with this inflammatory reaction resolving completely after 5 days. All animals gained weight, as expected: weight at day 30, 254 ± 9 g; weight at day 90, 319 ± 23 g (n = 18). At explantation, the constructs were easily retrieved, cohesive, and macroscopically well integrated in the surrounding tissues (Fig. S4) with no macroscopic signs of inflammation or other adverse reactions.

The cross-sectional dimensions of the implants in the two groups decreased by ~50% at day 30 as compared with their initial dimensions (ePTFE: −58%; and solid TNC: −46%); however, from day 30 to day 90, the cross-sectional area of both groups retained their dimensions (solid TNC: 6.5 ± 0.66 mm^2 and 7.7 ± 2.1 mm^2, respectively; and ePTFE: 4.2 ± 0.33 mm^2 and 4.15 ± 0.8 mm^2, respectively) (Table 6).

3.7. Histopathologic analysis of the implanted TNC hydrogels

In the 30-day groups, we observed no signs of necrosis, acute inflammation, or presence of polymorphonuclear cells in any of the samples; however, all samples displayed a foreign-body reaction with the presence of macrophages and giant cells (some containing engulfed biomaterial), as well as epithelioid cells and fibroblasts (Fig. 8). Notably, we found considerable internal variability in the groups, as well as between the four implants carried by the same individual. Additionally, the amount of degraded biomaterial and absorption varied between groups and within each group.

The TNC implants generally displayed abundant neovascularization, infiltrated connective tissue (i.e., granulation tissue), and a higher grade of biointegration activity as compared with the control group. Importantly, we identified abundant levels of giant cells and macrophages but no signs of acute inflammation (i.e., no polymorphonuclear leukocytes or degranulated mast cells) and only low-grade chronic inflammation (a low number of lymphocytes and plasma cells). Compared with the ePTFE controls, the foreign-body reaction was more diffuse and infiltrative, displaying both fat infiltration and a more indistinct border zone between the biomaterial and surrounding tissues.

Table 4
Storage modulus of alginate, TNC, and TNC/alginate hydrogels after cross-linking.

Sample	Storage modulus (Pa)
Alginate	10,948
TNC	3120
TNC/Alginate (80:20)	16,688.9

Measurements were taken at 10 min.

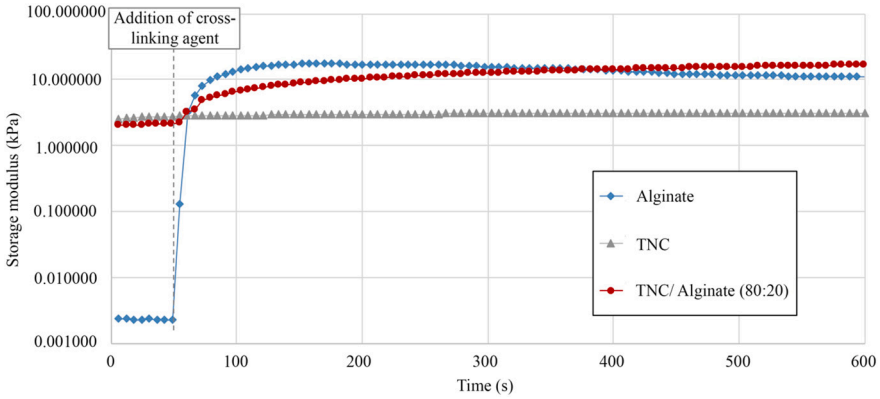

Fig. 6. Cross-linking ability. Storage modulus measured over time for alginate, TNC, and TNC/alginate (80:20) hydrogels using a rheometer. $CaCl_2$ cross-linking solution (1 ml; 100 mM) was added 60 s after initiating the measurement.

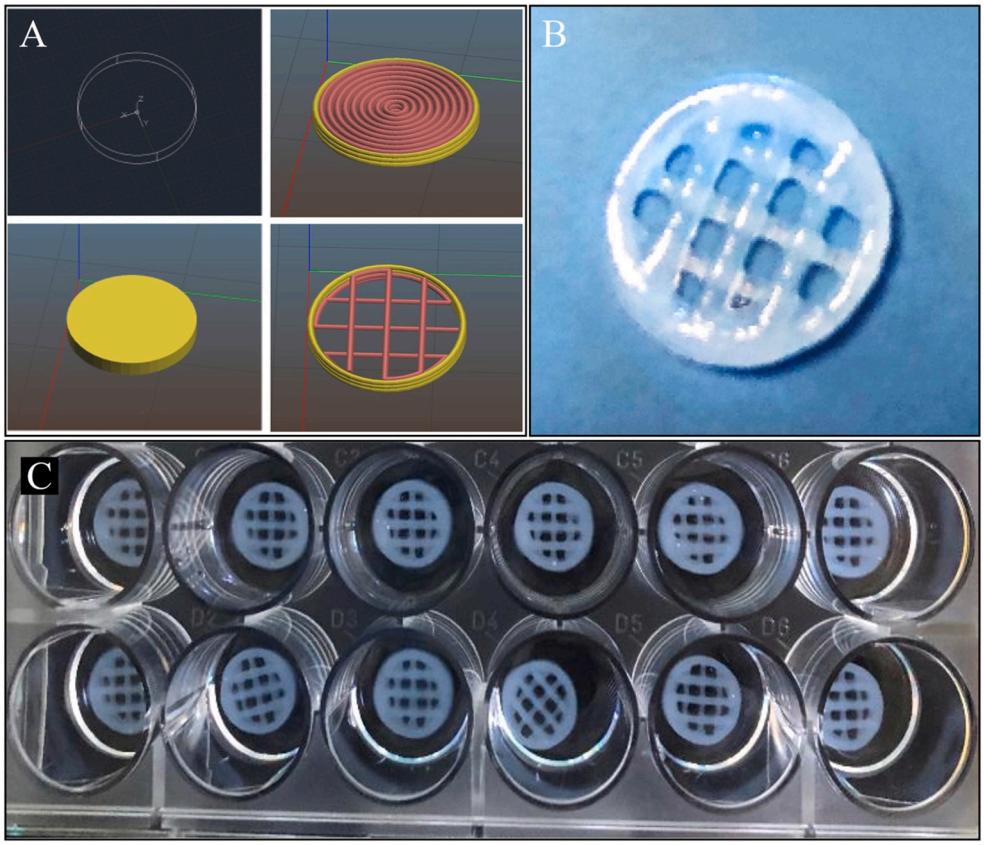

Fig. 7. Design of discs for the biocompatibility study. (A) Computer-aided design image showing the design of the solid and gridded discs. (B) A printed gridded disc from TNC/alginate hydrogel. (C) An array of printed gridded discs showing the reproducibility of the printing process. Printed discs were 10 mm in diameter and 1.2 mm in height.

Table 5
Average weight of the printed solid and gridded discs after cross-linking (n = 48).

Sample	Average weight after cross-linking (mg, mean ± SD)
Solid	110.0 ± 18.1
Grid	68.6 ± 3.9

Table 6
The average cross-sectional area of the constructs (a–d) in the four groups after 30 and 90 days.

Group	a	b	c	d	Average cross-sectional area (mm^2, mean ± SD)
ePTFE (day 30)	4.0	4.3	4.7	3.8	4.2 ± 0.3 (n = 12)
TNC (day 30)	6.8	5.7	6.1	7.4	6.5 ± 0.7 (n = 12)
ePTFE (day 90)	3.5	4.1	5.5	3.5	4.2 ± 0.8 (n = 12)
TNC (day 90)	4.4	7.5	9.3	9.5	7.7 ± 2.1 (n = 12)

Data for each group are presented as mm^2.

Semi-quantitative evaluation of biocompatibility according to ISO10993-6 resulted in a score corresponding to a "non-irritant" reaction as compared with that for ePTFE control (11.0 for the solid TNC implants and 9.3 for ePTFE) (Tables 7 and S2). Supplementary subanalyses are presented in Tables S4 and S6.

A notable difference detected between days 30 and 90 was the thicker capsule at day 90 in the ePTFE group. Additionally, the ePTFE material appeared less affected at day 90 as compared with the TNC implants, which demonstrated higher levels of phagocytosis. Moreover, we detected low-grade foreign-body-type inflammation (represented by lymphocytes and macrophages) in the TNC implants but no plasma cells or polymorphonuclear cells, and the surrounding capsule was thin and displayed almost no fibrosis. Moreover, in the TNC group, we observed more mature neovascularization (arterioles and venules) and prominent fat infiltration relative to the ePTFE controls (Figs. 9 and S5). Notably, we identified no infiltrates (fat or connective tissue) or neovascularization in the ePTFE constructs at any time point.

The ISO10993-6 assessment in the day 90 group resulted in a score corresponding to a "non-irritant" reaction (11.5 for the solid TNC implants and 9.4 for ePTFE) (Tables 8 and S3). Supplementary subanalyses are presented in Tables S5 and S7.

4. Discussion

Although TNC is comprised of >97% water, we found that it formed stable and resilient scaffolds with well-preserved and detailed fidelity. Structural comparisons between the TNC fibers and fibers extracted from wood showed that the TNC fibers could be manufactured in a more reproducible matter and with longer individual fibers. Additionally, TNC demonstrated tunable properties in terms of fiber length and viscosity by modulating the processing and changing its concentration in the hydrogels.

Moreover, the addition of alginate rendered the hydrogel cross-linkable, which is useful for 3D-bioprinting applications, where the hydrogel can be printed into various structures and then cross-linked with divalent cations for stable 3D constructs. Furthermore, the homogeneous nature of the fibers enables reproducible prints, and the tunable viscosity provides an alterable platform suitable for various applications. The printing fidelity was very high as displayed in Fig. 4C and D

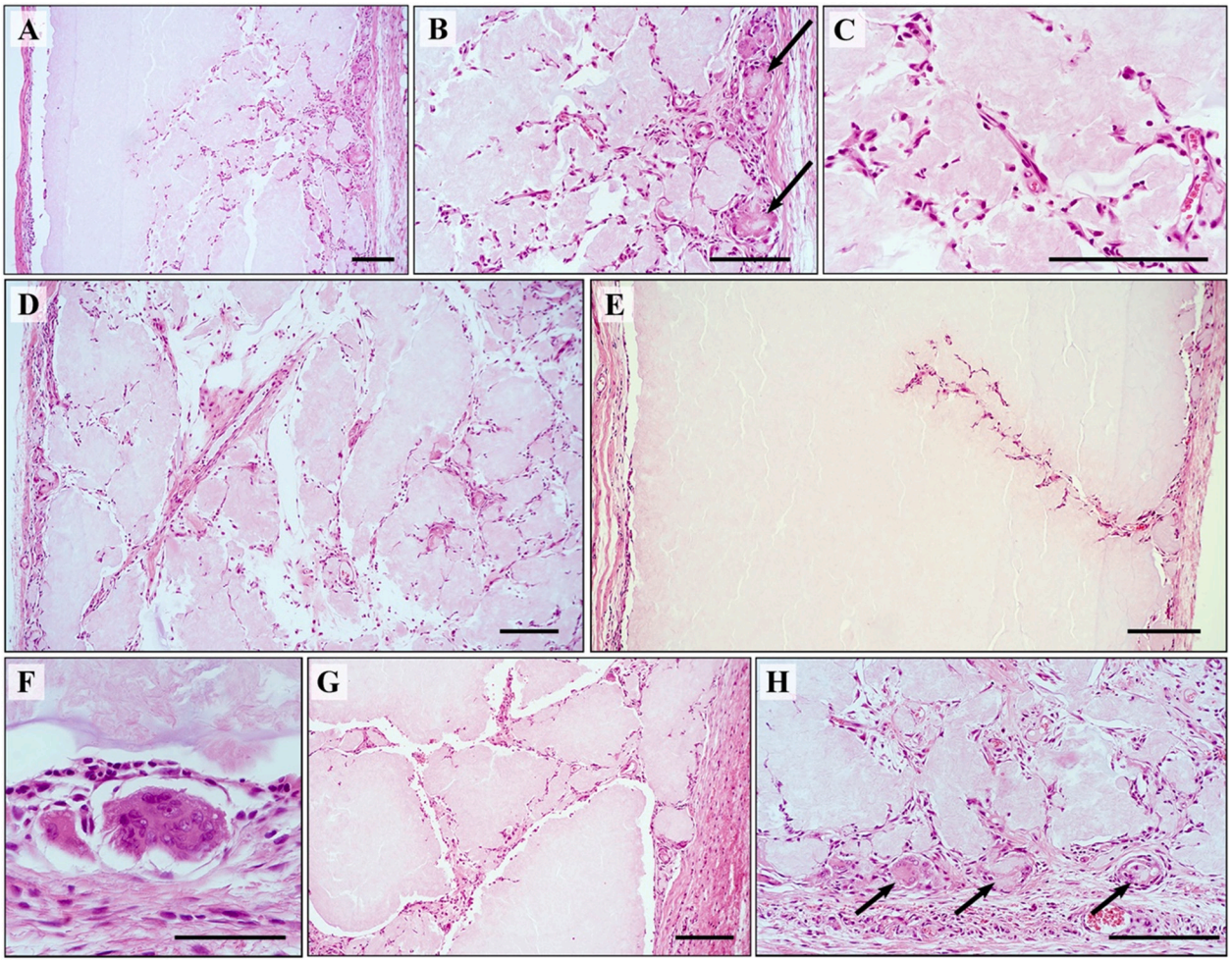

Fig. 8. Histopathologic analysis of the solid TNC implants at day 30. (A) Overview of vessel infiltration into the TNC biomaterial. (B) Magnification of the infiltrating vessels and giant cells (arrows) in the border zone. (C) Sprouting vessels. (D, E) Vessel infiltration in the TNC biomaterial. (F) A giant cell in the foreign-body reaction surrounding the TNC material. (G) Biomaterial fragmentation and vessel infiltration. (H) The border zone displaying an active foreign-body reaction and phagocytosis (arrows = giant cells). Bars, 200 μm (A–E and G–H) and 100 μm (F).

Table 7
Microscopic evaluation of TNC implants at day 30 according to ISO 10993-6 Annex E.

TNC d30 (n = 12)	Polymorphonuclear	Lymphocytes	Plasma cells	Macrophages	Giant cells	Necrosis	Subtotal (×2)	Neovascularization	Fibrosis	Fatty infiltrate	Total	Average (mean ± SD)
19a	0	1	0	2	2	0	10	2	1	0	13	11.0 ± 2.3
19b	0	1	0	1	1	0	6	2	1	0	9	
19c	0	1	0	1	1	0	6	2	1	0	9	
19d	0	1	0	1	1	0	6	1	1	0	8	
20a	0	2	0	1	1	0	8	3	1	0	12	
20b	0	1	0	2	1	0	8	3	1	0	12	
20c	0	1	0	1	1	0	6	1	1	0	8	
20d	0	1	0	1	1	0	6	2	1	0	9	
21a	0	2	0	2	2	0	12	2	1	0	15	
21b	0	2	0	2	1	0	10	3	1	0	14	
21c	0	1	0	2	2	0	10	2	1	0	13	
21d	0	1	0	1	1	0	6	3	1	0	10	

which shows printed grids with fibroblasts. The reproducibility of printing was very good (Fig. 7C and Table 5). The storage modulus of crosslinked TNC (10 min after crosslinking) was around 16 kPa. Testing of TNC/alginate hydrogels at different mixing ratios after crosslinking with $CaCl_2$ with unconfined compression showed similar force displacement curves as those reported by Markstedt et al. [45]. In that paper, nanocellulose derived from wood was mixed with alginate and at 30% compression displacement, the E modulus was around 100 kPa.

TNC is a novel nanocellulose-based biomaterial that had not previously been evaluated in vivo. In the present study, we determined that it is a highly-suitable and safe biomaterial with excellent rheological properties for applications with 3D-bioprinting technology. The chosen control biomaterial (ePTFE) has been used for decades as implants for many different purposes in humans and demonstrates excellent

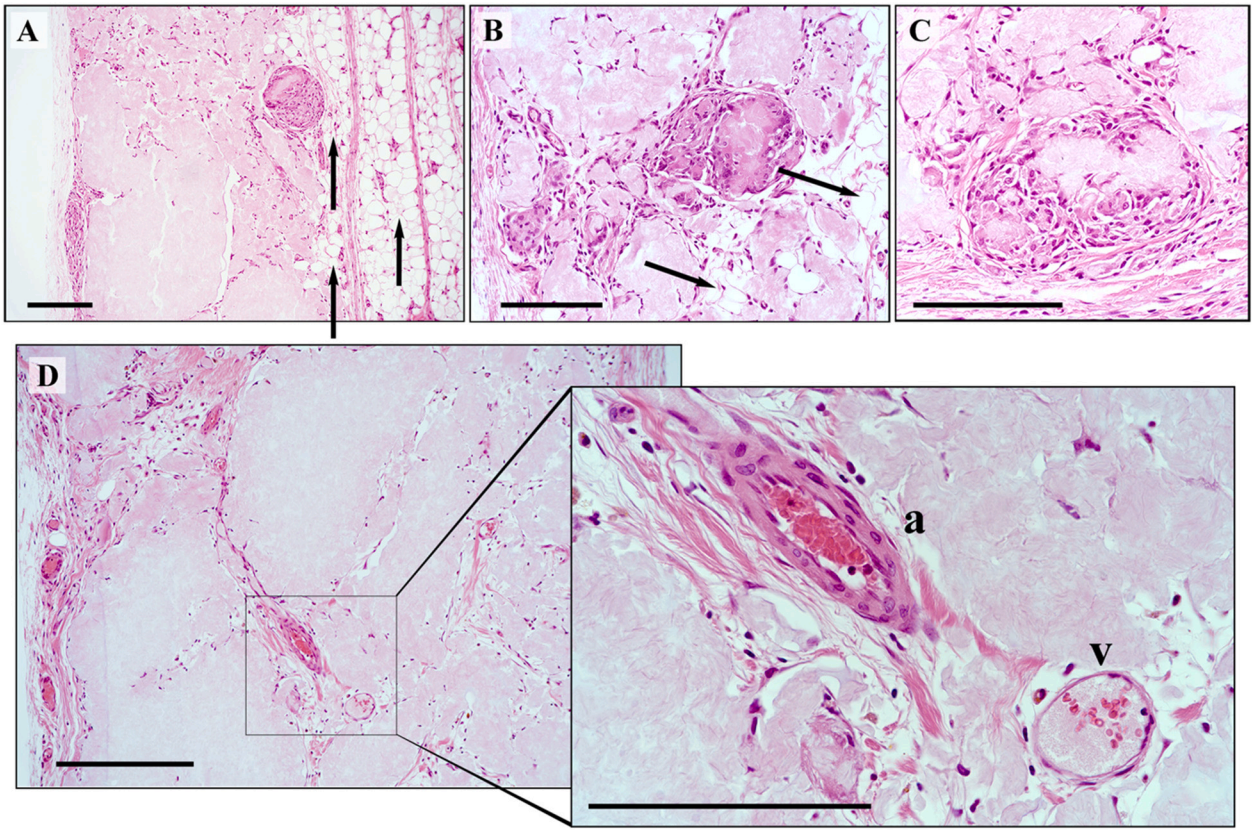

Fig. 9. Histopathologic analysis of solid TNC implants at day 90. (A) Overview of fat infiltration (arrows). (B) Fat infiltration (arrows). (C) Vessels and a giant cell phagocytosing the TNC biomaterial. (D) An arteriole (a) and a venule (v) inside the TNC biomaterial. Bars, 200 μm (A–D) and 100 μm in the magnification.

Table 8
Microscopic evaluation of TNC implants at day 90 according to ISO 10993-6 Annex E.

TNC d90 (n = 11)	Polymorphonuclear	Lymphocytes	Plasma cells	Macrophages	Giant cells	Necrosis	Subtotal (×2)	Neovascularization	Fibrosis	Fatty infiltrate	Total	Average (mean ± SD)
22a	0	1	0	1	1	0	6	2	1	1	10	11.5 ± 1.0
22b*	–	–	–	–	–	–	–	–	–	–	–	
22c	0	1	0	2	1	0	8	3	1	0	12	
22d	0	1	0	1	1	0	6	3	1	0	10	
23a	0	1	0	2	1	0	8	2	1	2	13	
23b	0	1	0	1	1	0	6	3	1	1	11	
23c	0	1	0	1	1	0	6	2	1	1	10	
23d	0	1	0	2	1	0	8	2	1	0	11	
24a	0	1	0	2	1	0	8	2	1	2	13	
24b	0	1	0	2	1	0	8	3	1	0	12	
24c	0	1	0	2	2	0	10	2	1	0	13	
24d	0	2	0	1	2	0	10	1	1	0	12	

* Damaged sample, evaluation uncertain.

biocompatibility [46–49]. Our hypothesis that TNC would initiate a mild foreign-body response comparable to that of ePTFE was corroborated by the ISO standardized analyses, which demonstrated that TNC engendered a low-grade inflammatory response and a high degree of biointegration. The ISO protocol require at least 10 samples each of the tested material and the control material, for comparison. We have used 12 solid TNC constructs, and 12 ePTFE controls for each time point.

In all groups, we identified a well-defined foreign-body reaction with large quantities of macrophages and giant cells. However, we did not find as much fibrosis as expected, as the encapsulating process generally yielded only a thin and disintegrated capsule of connective tissue. The reaction-zone area in the TNC construct was comparable to that in the ePTFE group, suggesting a similar level of immunological reaction. Previous studies showed that the TNC micromilieu subsidizes chondrogenesis and adipose tissue [50,51]. Although studies on other cell types or tissues have not yet been performed, the present findings suggest that from a biological standpoint, TNC likely offers a favorable environment for any cell type or tissue.

Comparisons of the cross-sectional areas added to the overall interpretation of the in vivo resilience of the biomaterial. The results suggested no large differences between TNC and ePTFE regarding degradation within 90 days. Discrepancies between the blinded area measurements were more frequent regarding the implants comprising more ingrowth in the biomaterial (i.e., the area with the most intense cell activity). It is possible that after 90 days, the intense biointegration process in the TNC construct will eventually bridge the degradation

observed in the biomaterial and progressively build up the new tissue. Although intended for a shorter time perspective, this principle has been previously applied to biodegradable bioinks.

Tunicate nanocellulose has previously been used as a scaffold in in vivo studies using nude mice [50–52]. In all these studies, TNC was mixed with alginate and crosslinked with Calcium ions prior to implantation. When the samples were mixed with cells we observed stable constructs, most probably due to production of extracellular matrix by cells. Nude mice lack cellular immunity, and are therefore not suitable for studies of biodegradation in humans. Cellulose is a robust molecule in comparison to other polysaccharides such as hyaluronic acid or alginate. In tunicates, cellulose is furthermore assembled into highly crystalline fibrils. The structure is similar to bacterial cellulose but the crystallinity is higher. TNC can be autoclaved or sterilized by radiation or electron beam which is a great advantage for use in tissue engineering. Cellulose is biodegradable by enzymes such as cellulase, but that enzyme is not present in humans [53]. There have been several studies requiring non-biodegradable properties that used bacterial cellulose as implants. We have previously reported 1 year patency of bacterial cellulose as vascular grafts in sheep [37]. Bacterial cellulose has also been used in clinical trials for repair of dura mater defects [54]. In summary, we anticipate that unmodified tunicate nanocellulose will not be rapidly degraded in the human body, making it suitable for biomedical implant durability. If degradability of the implant scaffold is desired in some applications, tunicate nanocellulose can be easily modified by for example oxidation, to make this biomaterial scaffold biodegradable.

Some of the TNC implants showed a dense cell count, and foreign-body activity, which made it challenging to discern a border between the implant and host tissue. The reaction-zone areas were intended for comparisons between the solid TNC group and the ePTFE control in order to assess differences in the foreign-body response. We found that the TNC biomaterial was more easily degraded and engulfed by macrophages than ePTFE; however, further analyses showed similar cross-sectional areas in both biomaterials (i.e., solid TNC and ePTFE), implying that the degradation, shrinkage, and consolidation processes were of the same magnitude. Additionally, both biomaterials retained their implant dimensions between days 30 and 90, suggesting that the degradation and macrophage activity declined after a more intense initial period. Furthermore, biointegration through infiltration of fat, connective tissue, and neovascularization was uncontested in the TNC groups. The penetrating neovascularization evident in the TNC constructs is highly interesting and will potentially bring tissue engineering a step closer to clinical translation. To address this, we recently investigated vascularization longitudinally over 3 months using magnetic resonance imaging [50,51]. To further evaluate this key issue, our next study will quantify the vascular structures and investigate the driving forces of vascularization (e.g., growth factors). Moreover, we plan to initiate analyses of the long-term features of TNC in studies that will include autologous chondrocytes capable of potentially building and restoring cartilaginous tissue and subsidized by the TNC biomaterial.

5. Conclusions

In this study, TNC has been demonstrated to possess several favorable features for usage in 3D-bioprinting. The mechanical properties are superior to nanocellulose extracted from other sources, and the biocompatibility is comparable to that of ePTFE.

Disclosure

Ocean TuniCell AS (C.T., and E.M.T.) markets tunicate nanocellulose products but did not participate or influence in any way the independent ISO10993-6 evaluations carried out by surgeons and pathologists at the Sahlgrenska University Hospital.

P.A., L.K., K.S., J.M., P.G., and S.S. have no competing financial interests to declare in relation to the content of this article.

CRediT author statement

C.T., and E.M.T. managed the TNC production chain and conducted/interpreted the biomaterial characterizations. P.A., S.S., K.S., P.G., and L.K. designed the in vivo study and performed the experiments. S.S. did the in vitro experiments and all the 3D bioprinting procedures. P.A., K.S., J.M. and L.K. analyzed and interpreted the histological data. P.A., K.S., and L.K. wrote the biocompatibility sections and C.T., E.M.T., S.S., and P.G. wrote the biomaterial sections.

CRediT authorship contribution statement

Writing - original draft: Peter Apelgren, Eric M.Thompson, Christofer Troedsson, Lars Kölby, Sanna Sämfors, Paul Gatenholm.

Writing - review & editing: Peter Apelgren, Eric M.Thompson, Christofer Troedsson, Lars Kölby, Karin Säljö, Sanna Sämfors, Paul Gatenholm.

Declaration of competing interest

Ocean TuniCell AS (C.T., and E.M.T.) markets tunicate nanocellulose products but did not participate or influence in any way the independent ISO10993-6 evaluations carried out by surgeons and pathologists at the Sahlgrenska University Hospital. P.A., L.K., K.S., J.M., P.G., and S.S have no competing financial interests to declare in relation to the content of this article.

Acknowledgments

We would like to express our gratitude to Dr. Linnea Stridh Orrhult for help with fibroblast bioprinting and viability evaluation. Additionally, we would like to thank Anders Mårtensson for help with AFM analysis. This study was partially supported by grants from the Research Council of Norway (IPN-317790/F20 to E.M.T., C.T., and P.G.) and the Research Council of Sweden (2021-00971 to L.K.). This work was also supported by Sahlgrenska University Hospital and Sahlgrenska Academy at the University of Gothenburg and financed by grants from the Swedish state under the ALF agreement between the Swedish government and the County Councils (ALFGBG-716621 and ALFGBG-965533). The Knut and Alice Wallenberg Foundation provided financial support in the framework of the Wallenberg Wood Science Center and this study was also supported by grants from the Gothenburg Medical Society, the Wilhelm and Martina Lundgren Foundation for Science, the Mary von Sydow Foundation, the Magnus Bergvalls Foundation, the Sigurd and Elsa Goljes Foundation, and the Ann-Mari and Per Ahlqvist Foundation.

Appendix A. Supplementary data

Supplementary data to this article can be found online at https://doi.org/10.1016/j.bioadv.2022.212828.

References

[1] H. Backdahl, G. Helenius, A. Bodin, U. Nannmark, B.R. Johansson, B. Risberg, P. Gatenholm, Mechanical properties of bacterial cellulose and interactions with smooth muscle cells, Biomaterials 27 (2006) 2141–2149.
[2] H. Ahrem, D. Pretzel, M. Endres, D. Conrad, J. Courseau, H. Müller, R. Jaeger, C. Kaps, D.O. Klemm, R.W. Kinne, Laser-structured bacterial nanocellulose hydrogels support ingrowth and differentiation of chondrocytes and show potential as cartilage implants, Acta Biomater. 10 (2014) 1341–1353.
[3] H. Martínez Ávila, E.M. Feldmann, M.M. Pleumeekers, L. Nimeskern, W. Kuo, W. C. de Jong, S. Schwarz, R. Müller, J. Hendriks, N. Rotter, G.J. van Osch, Novel bilayer bacterial nanocellulose scaffold supports neocartilage formation in vitro and in vivo, Biomaterials 44 (2015) 122–133.
[4] L. Nimeskern, H. Martínez Ávila, J. Sundberg, P. Gatenholm, R. Müller, K.S. Stok, Mechanical evaluation of bacterial nanocellulose as an implant material for ear cartilage replacement, J. Mech. Behav. Biomed. Mater. 22 (2013) 12–21.
[5] H. Martínez Ávila, S. Schwarz, E.M. Feldmann, A. Mantas, A. von Bomhard, P. Gatenholm, N. Rotter, Biocompatibility evaluation of densified bacterial

nanocellulose hydrogel as an implant material for auricular cartilage regeneration, Appl. Microbiol. Biotechnol. 98 (2014) 7423–7435.
[6] Y. Sagane, K. Zech, J.M. Bouquet, M. Schmid, U. Bal, E.M. Thompson, Functional specialization of cellulose synthase genes of prokaryotic origin in chordate larvaceans, Development 137 (2010) 1483–1492.
[7] P.S. Belton, S.F. Tanner, N. Cartier, H. Chanzy, High-resolution solid-state C-13 nuclear magnetic-resonance spectroscopy of tunicin, an animal cellulose, Macromolecules 22 (1989) 1615–1617.
[8] S. Kimura, T. Itoh, New cellulose synthesizing complexes (terminal complexes) involved in animal cellulose biosynthesis in the tunicate Metandrocarpa uedai, Protoplasma 194 (1996) 151–163.
[9] L. Brinchi, F. Cotana, E. Fortunati, J.M. Kenny, Production of nanocrystalline cellulose from lignocellulosic biomass: technology and applications, Carbohyd Polym 94 (2013) 154–169.
[10] M.J. Dunlop, B. Acharya, R. Bissessur, Study of plant and tunicate based nanocrystalline cellulose in hybrid polymeric nanocomposites, Cellulose 27 (2020) 249–261.
[11] Y.D. Zhao, J.B. Li, Excellent chemical and material cellulose from tunicates: diversity in cellulose production yield and chemical and morphological structures from different tunicate species, Cellulose 21 (2014) 3427–3441.
[12] P. Apelgren, E. Karabulut, M. Amoroso, A. Mantas, H. Martínez Ávila, L. Kölby, T. Kondo, G. Toriz, P. Gatenholm, In vivo human cartilage formation in three-dimensional bioprinted constructs with a novel bacterial nanocellulose bioink, Acs Biomater Sci Eng 5 (2019) 2482–2490.
[13] Y.D. Zhao, Y.J. Zhang, M.E. Lindstrom, J.B. Li, Tunicate cellulose nanocrystals: preparation, neat films and nanocomposite films with glucomannans, Carbohyd Polym 117 (2015) 286–296.
[14] W. Pustlauk, B. Paul, M. Gelinsky, A. Bernhardt, Jellyfish collagen and alginate: combined marine materials for superior chondrogenesis of hMSC, Mat Sci Eng C-Mater 64 (2016) 190–198.
[15] S. Kimura, T. Itoh, Cellulose synthesizing terminal complexes in the ascidians, Cellulose 11 (2004) 377–383.
[16] P. Ward, Acute and chronic inflammation, in: S. Ayoub, C. Serhan, P. Ward, D. Gilroy (Eds.), Fundamentals of Inflammation 1-16, Cambridge University Press, 2010.
[17] J.M. Anderson, A. Rodriguez, D.T. Chang, Foreign body reaction to biomaterials, Semin Immunol 20 (2008) 86–100.
[18] T. Albrektsson, T. Jemt, J. Mölne, P. Tengvall, A. Wennerberg, On inflammation-immunological balance theory-a critical apprehension of disease concepts around implants: mucositis and marginal bone loss may represent normal conditions and not necessarily a state of disease, Clin. Implant. Dent. Relat. Res. 21 (2019) 183–189.
[19] G. Voskerician, R.S. Shawgo, P.A. Hiltner, J.M. Anderson, M.J. Cima, R. Langer, In vivo inflammatory and wound healing effects of gold electrode voltammetry for MEMS micro-reservoir drug delivery device, Ieee T Bio-Med Eng 51 (2004) 627–635.
[20] G. Voskerician, P.H. Gingras, J.M. Anderson, Macroporous condensed poly (tetrafluoroethylene). I. In vivo inflammatory response and healing characteristics, J Biomed Mater Res A 76a (2006) 234–242.
[21] I. Kolesnik, T. Tverdokhlebova, N. Danilenko, E. Plotnikov, D. Kulbakin, A. Zheravin, V. Bouznik, E. Bolbasov, Characterization and determination of the biocompatibility of porous polytetrafluoroethylene membranes fabricated via electrospinning, J Fluorine Chem 246 (2021).
[22] A.J.T. Teo, A. Mishra, I. Park, Y.J. Kim, W.T. Park, Y.J. Yoon, Polymeric biomaterials for medical implants and devices, Acs Biomater Sci Eng 2 (2016) 454–472.
[23] I. Kondyurina, I. Shardakov, G. Nechitailo, V. Terpugov, A. Kondyurin, Cell growing on ion implanted polytetrafluorethylene, Appl. Surf. Sci. 314 (2014) 670–678.
[24] D.A. Jacob, C. Schug-Pass, F. Sommerer, A. Tannapfel, H. Lippert, F. Köckerling, Comparison of a lightweight polypropylene mesh (Optilene (R) LP) and a large-pore knitted PTFE mesh (GORE (R) INFINIT (R) mesh)-biocompatibility in a standardized endoscopic extraperitoneal hernia model, Langenbeck Arch Surg 397 (2012) 283–289.
[25] L.N. Fu, J. Zhang, G. Yang, Present status and applications of bacterial cellulose-based materials for skin tissue repair, Carbohyd Polym 92 (2013) 1432–1442.
[26] D.J. Modulevsky, C.M. Cuerrier, A.E. Pelling, Biocompatibility of subcutaneously implanted plant-derived cellulose biomaterials, PLoS One 11 (2016), e0157894.
[27] D.J. Modulevsky, C. Lefebvre, K. Haase, Z. Al-Rekabi, A.E. Pelling, Apple-derived cellulose scaffolds for 3D mammalian cell culture, PLoS One 9 (2014), e97835.
[28] N. Contessi Negrini, N. Toffoletto, S. Farè, L. Altomare, Plant tissues as 3D natural scaffolds for adipose, bone and tendon tissue regeneration, Front Bioeng Biotech 8 (2020), 723.
[29] M. Osorio, A. Cañas, J. Puerta, L. Díaz, T. Naranjo, I. Ortiz, C. Castro, Ex vivo and in vivo biocompatibility assessment (blood and tissue) of three-dimensional bacterial nanocellulose biomaterials for soft tissue implants, Sci Rep 9 (2019) 10553.
[30] P. Apelgren, M. Amoroso, A. Lindahl, C. Brantsing, N. Rotter, P. Gatenholm, L. Kölby, Chondrocytes and stem cells in 3D-bioprinted structures create human cartilage in vivo, PLoS One 12 (2017), e0189428.
[31] P. Apelgren, M. Amoroso, K. Säljö, A. Lindahl, C. Brantsing, L. Stridh Orrhult, K. Markstedt, P. Gatenholm, L. Kölby, Long-term in vivo integrity and safety of 3D-bioprinted cartilaginous constructs, J Biomed Mater Res B 109 (2021) 128–136.
[32] P. Apelgren, M. Amoroso, K. Säljö, A. Lindahl, C. Brantsing, L. Stridh Orrhult, P. Gatenholm, L. Kölby, Skin grafting on 3D bioprinted cartilage constructs in vivo, Plast Reconstr Surg Glob Open 6 (2018), e1930.
[33] A. Bodin, S. Concaro, M. Brittberg, P. Gatenholm, Bacterial cellulose as a potential meniscus implant, J. Tissue Eng. Regen. Med. 1 (2007) 406–408.
[34] G. Chinga-Carrasco, Potential and limitations of nanocelluloses as components in biocomposite inks for three-dimensional bioprinting and for biomedical devices, Biomacromolecules 19 (2018) 701–711.
[35] G. Chinga-Carrasco, N.V. Ehman, J. Pettersson, M.E. Vallejos, M.W. Brodin, F. E. Felissia, J. Håkansson, M.C. Area, Pulping and pretreatment affect the characteristics of bagasse inks for three-dimensional printing, Acs Sustain Chem Eng 6 (2018) 4068–4075.
[36] D. Klemm, D. Schumann, U. Udhardt, S. Marsch, Bacterial synthesized cellulose - artificial blood vessels for microsurgery, Prog. Polym. Sci. 26 (2001) 1561–1603.
[37] C.J. Malm, B. Risberg, A. Bodin, H. Bäckdahl, B.R. Johansson, P. Gatenholm, A. Jeppsson, Small calibre biosynthetic bacterial cellulose blood vessels: 13-months patency in a sheep model, Scand Cardiovasc J 46 (2012) 57–62.
[38] M. Ojansivu, A. Rashad, A. Ahlinder, J. Massera, A. Mishra, K. Syverud, A. Finne-Wistrand, S. Miettinen, K. Mustafa, Wood-based nanocellulose and bioactive glass modified gelatin-alginate bioinks for 3D bioprinting of bone cells, Biofabrication 11 (2019).
[39] A. Shavandi, S. Hosseini, O.V. Okoro, L. Nie, F.E. Babadi, F. Melchels, 3D bioprinting of lignocellulosic biomaterials, Adv. Healthcare Mater. 9 (2020), e2001472.
[40] A. Svensson, E. Nicklasson, T. Harrah, B. Panilaitis, D.L. Kaplan, M. Brittberg, P. Gatenholm, Bacterial cellulose as a potential scaffold for tissue engineering of cartilage, Biomaterials 26 (2005) 419–431.
[41] M. Zaborowska, A. Bodin, H. Bäckdahl, J. Popp, A. Goldstein, P. Gatenholm, Microporous bacterial cellulose as a potential scaffold for bone regeneration, Acta Biomater. 6 (2010) 2540–2547.
[42] D. Kim, J. Jeong, J.A. Ryu, S.R. Choi, J.M. Lee, H. Bunch, In vitro evaluation of lignin-containing nanocellulose, Materials (Basel) 13 (2020) 3365.
[43] N. Lin, A. Dufresne, Nanocellulose in biomedicine: current status and future prospect, Eur. Polym. J. 59 (2014) 302–325.
[44] S. Park, J.O. Baker, M.E. Himmel, P.A. Parilla, D.K. Johnson, Cellulose crystallinity index: measurement techniques and their impact on interpreting cellulase performance, Biotechnol Biofuels 3 (2010).
[45] K. Markstedt, A. Mantas, I. Tournier, H. Martínez Ávila, D. Hägg, P. Gatenholm, 3D bioprinting human chondrocytes with nanocellulose-alginate bioink for cartilage tissue engineering applications, Biomacromolecules 16 (2015) 1489–1496.
[46] International Organization for Standardizationcollab <collab>ISO, Part 6: Tests for Local Effects After Implantation, 2016. Annex E, Geneva.
[47] M. Deutsch, J. Meinhart, P. Zilla, N. Howanietz, M. Gorlitzer, A. Froeschl, A. Stuempflen, D. Bezuidenhout, M. Grabenwoeger, Long-term experience in autologous in vitro endothelialization of infrainguinal ePTFE grafts, J. Vasc. Surg. 49 (2009) 352–362.
[48] P.P. Caimmi, M. Sabbatini, L. Fusaro, A. Borrone, M. Cannas, A study of the mechanical properties of ePTFE suture used as artificial mitral chordae, J Cardiac Surg 31 (2016) 498–502.
[49] N. Takahashi, Y. Suzuki, H. Ujiie, T. Hori, M. Iwaki, T. Yamada, Biocompatibility of modified ePTFE for an artificial dura mater, Nucl Instrum Meth B 242 (2006) 61–64.
[50] P. Apelgren, M. Amoroso, K. Säljö, M. Montelius, A. Lindahl, L. Strid Orrhult, P. Gatenholm, L. Kölby, Vascularization of tissue engineered cartilage - sequential in vivo MRI display functional blood circulation, Biomaterials 276 (2021), 121002.
[51] M. Amoroso, P. Apelgren, K. Säljö, M. Montelius, L. Strid Orrhult, M. Engström, P. Gatenholm, L. Kölby, Functional and morphological studies of in vivo vascularization of 3D bioprinted human fat grafts, Bioprinting 23 (2021), e00162.
[52] K. Säljö, P. Apelgren, L. Orrhult Stridh, S. Li, P. Gatenholm, L. Kölby, Long-term in vivo survival of 3D-bioprinted human lipoaspirate-derived adipose tissue: proteomic signature and cellular content, Adipocyte 11 (1) (2022) 34–46.
[53] S. Torgbo, P. Sukyai, Biodegradation and thermal stability of bacterial cellulose as biomaterial: the relevance in biomedical applications, Polym. Degrad. Stab. 179 (2020), 109232.
[54] C.L. Rosen, G.K. Steinberg, F. DeMonte, J.B. Delashaw, S.B. Lewis, M.E. Shaffrey, K. Aziz, J. Hantel, F.F. Marciano, Results of the prospective, randomized, multicenter clinical trial evaluating a biosynthesized cellulose graft for repair of dural defects, Neurosurgery 69 (2011) 1093–1103.